The Astrophysical Journal, 642:1275–1285, 2006 May 10

DIELECTRONIC RECOMBINATION OF Fe XXIII FORMING Fe XXII: LABORATORY MEASUREMENTS AND THEORETICAL CALCULATIONS

D. W. Savin
Columbia Astrophysics Laboratory, Columbia University, 550 West 120th Street, Mail Code 5247, New York, NY 10027;
savin@astro.columbia.edu

G. Gwinner,[1] M. Grieser, R. Repnow, M. Schnell,[2] D. Schwalm, A. Wolf, and S.-G. Zhou[3]
Max-Planck-Institut für Kernphysik, Saupfercheckweg 1, Postfach 10 39 80, D-69117 Heidelberg, Germany

S. Kieslich, A. Müller, and S. Schippers
Institut für Atom- und Molekülphysik, Justus-Liebig-Universität, D-35392 Giessen, Germany

J. Colgan
Los Alamos National Laboratory, P.O. Box 1663, Los Alamos, NM 87545

S. D. Loch
Physics Department, Auburn University, 206 Allison Laboratory, Auburn, AL 36849

N. R. Badnell
Department of Physics, University of Strathclyde, Glasgow G4 0NG, UK

M. H. Chen
Lawrence Livermore National Laboratory, P.O. Box 808, Livermore, CA 94551

and

M. F. Gu
Department of Physics and Kavli Institute for Particle Astrophysics and Cosmology,
Stanford University, 382 Via Pueblo Mall, Stanford, CA 94305
Received 2005 July 8; accepted 2006 January 15

ABSTRACT

We have measured resonance strengths and energies for dielectronic recombination (DR) of beryllium-like Fe XXIII forming boron-like Fe XXII via $N = 2 \rightarrow N' = 2$ and $N = 2 \rightarrow N' = 3$ core excitations. All measurements were carried out using the heavy-ion Test Storage Ring at the Max Planck Institute for Nuclear Physics (MPI-K) in Heidelberg, Germany. We have also calculated these resonance strengths and energies using three independent, perturbative, state-of-the-art theoretical techniques: the multiconfiguration Breit-Pauli (MCBP) method, the multiconfiguration Dirac-Fock (MCDF) method, and the Flexible Atomic Code (FAC). Overall reasonable agreement is found between our experimental results and these theoretical calculations. We have used our measurements to produce a Maxwellian-averaged DR rate coefficient for Fe XXIII. Our experimentally derived rate coefficient is estimated to be accurate to better that ≈20%. At temperatures where Fe XXIII is predicted to form in both photoionized and electron-ionized gas, we find mixed agreement between our experimental rate coefficient and previously published rate coefficients. We find good agreement at these temperatures between the experimentally derived rate coefficient and our MCBP, MCDF, and FAC results.

Subject headings: atomic data — atomic processes

1. INTRODUCTION

Dielectronic recombination (DR) is an important recombination process in both photoionized and electron-ionized plasmas (Ferland et al. 1998; Mazzotta et al. 1998). Accurate DR data are needed to interpret and model the line emission, thermal structure, and ionization structures of these plasmas (Mewe et al. 1985; Brickhouse et al. 1995; Ferland et al. 1998; Savin et al. 1999, 2000). Laboratory measurements can provide a small portion of the needed DR rate coefficients. But theoretical calculations are used to produce the bulk of the required DR data (Ferland et al. 1998; Mazzotta et al. 1998; Kallman & Bautista 2001). The accuracy of the theoretical DR data is thus an issue of major concern (Ferland 2003). Laboratory measurements play an important role in benchmarking theory, testing its accuracy, and improving our understanding of the DR process. But in instances where theory is not able to accurately calculate the relevant DR resonance structure and energies, laboratory measurements are the only way to produce reliable DR rate coefficients.

DR is a two-step recombination process that begins when a free electron approaches an ion, collisionally excites a bound electron of the ion, and is simultaneously captured. The electron excitation can be labeled $Nl_j \rightarrow N'l'_{j'}$, where N is the principal quantum number of the core electron, l is its orbital angular momentum, and j is its total angular momentum. The intermediate state, formed by simultaneous excitation and capture, may autoionize. The DR process is complete when the intermediate state emits a photon that reduces the total energy of the recombined ion to below its ionization limit. Conservation of energy requires that for DR to go forward $E_k = \Delta E - E_b$. Here E_k is the

[1] Current address: Department of Physics and Astronomy, University of Manitoba, Winnipeg, MB R3T 2N2, Canada.
[2] Current address: Columbia Astrophysics Laboratory, Columbia University, New York, NY 10027.
[3] Current address: School of Physics, Peking University, Beijing 100871, China.

kinetic energy of the incident electron, ΔE is the excitation energy of the initially bound electron in the presence of the captured electron, and E_b is the binding energy released when the incident electron is captured onto the excited ion. Because ΔE and E_b are quantized, DR is a resonant process.

The strength of a DR resonance is given by the integral of the resonance cross section over energy. In the isolated resonance approximation, the integrated strength of a particular DR resonance S_d can be approximated as (Kilgus et al. 1992)

$$S_d = \frac{h\mathcal{R}}{E_d}\pi a_0^2 \frac{g_d}{2g_i}\frac{A_a(d \rightarrow i)\sum_f A_r(d \rightarrow f)}{\sum_\kappa A_a(d \rightarrow \kappa) + \sum_{f'} A_r(d \rightarrow f')}. \quad (1)$$

Here h is the Planck constant, $\mathcal{R}$ is the Rydberg energy constant, E_d is the energy of resonance d, a_0 is the Bohr radius, g_d and g_i are the statistical weights of d and of the initial ion, respectively, A_a and A_r are the autoionization and radiative decay rates, respectively, $\sum_f$ is over all states stable against autoionization, $\sum_{f'}$ is over all states energetically below d, both $\sum_f$ and $\sum_{f'}$ may include cascades through lower lying autoionizing states and ultimately to bound states, and $\sum_\kappa$ is over all states attainable by autoionization of d. Rate coefficients for plasma modeling are produced by multiplying S_d with the relative electron-ion velocity, integrating over a Maxwellian electron energy distribution, and then summing the contributions due to all resonances d.

Theoretical DR rate coefficients for K-shell ions are believed to be well understood. This is partially due to a sustained series of electron beam ion trap (EBIT) and ion storage ring measurements over the past 15 yr. These measurements have provided important benchmarks for the development of modern theoretical methods for calculating DR. Comparisons of experimental and theoretical K-shell DR studies have been reviewed by Müller (1995) and Savin & Laming (2002). Overall agreement between state-of-the-art theory and experiment is on the order of $\sim$20%.

The situation for L-shell ions, however, has not been so good. Until recently the published L-shell DR data have been highly unreliable. For example, laboratory measurements of DR for L-shell ions have found factors of 2 to order-of-magnitude errors in the published DR rate coefficients (Savin et al. 1997, 1999, 2002a, 2002b, 2003; Schippers et al. 2000, 2001, 2004). For ions where there are no measurements, published theoretical results can differ from one another by factors of 2 or more (Arnaud & Raymond 1992; Savin 2000; Savin & Laming 2002).

However, in the last year or so the quality of the theoretical DR data available for modeling cosmically abundant L-shell ions has changed significantly. State-of-the-art theoretical results are now being systematically published for a wide range of cosmically abundant elements (e.g., Badnell et al. 2003; Chen 2002; Gu 2003b; Zatsarinny et al. 2003). The reliability of these calculations has been greatly helped by a concerted series of benchmark measurements using ion storage rings over the past 10+ yr. This paper is part of that DR effort.

In an attempt to provide reliable DR data for plasma modeling, storage ring measurements have been carried out for a wide range of L-shell ions. In order best to test theory, it is important to have laboratory results for every isoelectronic sequence at both the low- and high-Z ends of the range in atomic number Z for which data are needed. In this way one can test the theoretical and computational approximations used and determine their reliability as a function of Z over the range of interest.

Covering all of the cosmically abundant elements requires data up to $Z = 30$. Hence, within this range it is useful to note the lowest and highest Z ions in each L-shell isoelectronic sequence for which ion storage ring measurements exist. We adopt the labeling convention here of using the charge state of the ion before undergoing DR.

Measurements of $2 \rightarrow 2$ DR exist for a number of Li-like ions from Be^+ (Mohamed et al. 2002) to Cu^{26+} (Kilgus et al. 1992). We also note the high-resolution, single-pass, merged-beams measurement for Ar^{15+} of Schennach et al. (1994). For Be-like ions measurements have been carried out for a number of systems from C^{2+} (Fogle et al. 2005) to Cu^{25+} (M. Schnell et al. 2006, in preparation; see also Schnell et al. 2003). For B-like ions, storage ring measurements exist for Ar^{13+} (DeWitt et al. 1996) and Fe^{21+} (Savin et al. 2003). For C-like, N-like, and O-like systems, the only storage ring measurements we are aware of are those on Fe^{20+} (Savin et al. 2003), Fe^{19+} (Savin et al. 2002b), and Fe^{18+} (Savin et al. 1999, 2002a), respectively. And lastly, storage ring results have been published for F-like Fe^{17+} (Savin et al. 1997, 1999) and for the higher Z ion Se^{25+} (Lampert et al. 1996) but not for any lower Z systems.

The situation for storage ring measurements of $2 \rightarrow 3$ DR is much spottier. Results have been published for Li-like Si^{11+} (Kenntner et al. 1995) and Cu^{26+} (Kilgus et al. 1992). Again, it is worth noting the work on Ar^{15+} by Schennach et al. (1994). For Be-like, O-like, and F-like ions, the only measurements we are aware of are, respectively, those for Mg^{8+} (Schippers et al. 2004), Fe^{18+} (Savin et al. 2002a), and F-like Se^{25+} (even though this is above our $Z = 30$ cutoff; Lampert et al. 1996). We are unaware of any $2 \rightarrow 3$ storage ring DR measurements for ions in the B-like, C-like, N-like, or Ne-like isoelectronic sequences.

These and other storage ring measurements of L-shell DR have done much to improve the quality of state-of-the-art DR calculations. However, important issues remain unresolved. For example, $2 \rightarrow 2$ resonances dominate the DR process at low energies. But state-of-the-art theory is still unable to predict reliably the position of near zero energy DR resonances. For ions that form at temperatures where these low-energy resonances are important, this can result in a factor of 2 or more difference between theory and experiment (Schippers et al. 2004). Clearly an improvement is needed in the atomic structure codes used to calculate the relevant DR resonance energies. A second unresolved issue is the reliability of modern DR calculations for $2 \rightarrow 3$ core excitations. These calculations have been benchmarked for only a few ions in four of the L-shell isoelectronic sequences. For the other four sequences no measurements at all exist. Lastly, for $2 \rightarrow 2$ and $2 \rightarrow 3$ DR there are many isoelectronic sequences for which measurements do not span the range of important ions but rather exist for only a single ion. It is clear that further laboratory work is still needed to benchmark L-shell DR calculations for DR via both of these core excitations.

Here we present recent laboratory results for $2 \rightarrow 2$ and $2 \rightarrow 3$ DR of Fe XXIII forming Fe XXII. DR via $2 \rightarrow 2$ core excitations can proceed via the following resonances:

$$\mathrm{Fe}^{22+}\left[2s^2\left({}^1S_0\right)\right] + e^- \rightarrow \left\{ \begin{array}{c} \mathrm{Fe}^{21+}\left[2s2p\left({}^3P^o_{0,1,2};\ {}^1P^o_1\right)nl\right] \\ \mathrm{Fe}^{21+}\left[2p^2\left({}^3P_{0,1,2};\ {}^1D_2;\ {}^1S_0\right)nl\right] \end{array} \right\}. \quad (2)$$

In our studies we measured $2 \rightarrow 2$ DR resonances for electron-ion collision energies between 0 and $\approx$98 eV. For $2 \rightarrow 3$ DR we have carried out measurements for recombination via the capture channels:

$$\mathrm{Fe}^{22+}\left[2s^2\left({}^1S_0\right)\right] + e^- \rightarrow \mathrm{Fe}^{21+}(2s3lnl'). \quad (3)$$

These measurements have been carried for energies between ≈230 and 1240 eV. There are no significant DR resonances predicted between ≈98 and 230 eV.

This paper is organized as follows: The experimental arrangement for our measurements is described in § 2. Our laboratory results are presented in § 3. Theoretical calculations that have been carried out for comparison with our results are discussed in § 4. Comparisons between experimental and theoretical results are presented in § 5.

2. EXPERIMENTAL TECHNIQUE

Our laboratory studies have been performed using the heavy-ion Test Storage Ring (TSR) at the Max-Planck-Institute for Nuclear Physics in Heidelberg, Germany. DR measurements are carried out by merging, in one of the straight sections of TSR, a circulating ion beam with an electron beam for a distance of ≈1.5 m. The electrons are demerged from the primary and recombined ion beams using toroidal magnets. After demerging, recombined ions are separated from the stored ions using a dipole magnet and directed onto a detector. The relative electron-ion collision energy can be precisely controlled and the recombination signal measured as a function of this energy. Details of the experimental setup have been given elsewhere (Kilgus et al. 1992; Lampert et al. 1996; Schippers et al. 1998, 2000, 2001).

After demerging from the electron beam, the primary and recombined ions pass through two correction dipole magnets. Both beams then pass through a dipole that separates the recombined ions from the primary ion beam and directs the recombined ions onto a detector. Some of the recombined ions can be field ionized by motional electric fields before the detector and thus are not detected. Field ionization of the recombined ions passing through these three sets of magnets has been modeled by Schippers et al. (2001). Their formalism uses the hydrogenic approximation to take into account the radiative lifetime of the Rydberg level into which the initially free electron is captured. Using this methodology, we estimate for Fe XXIII that electrons captured into $n_{\max} \lesssim 118$ are detected by our experimental arrangement.

For the DR measurements reported here, a beam of $^{56}Fe^{22+}$ was produced by the tandem accelerator and rf linear accelerator at the Max-Planck-Institute for Nuclear Physics by stripping a beam of iron ions in a carbon foil at the energy of the maximum equilibrium yield for charge state 22+ (Shima et al. 1992). The beam was then injected into the storage ring at an energy of 248 MeV. The initial energy spread of the ions was reduced using standard electron cooling techniques. In cooling mode the electron beam current was 80 mA with a radius of 3 cm. The ion beam can heat up due to intrabeam scattering. The size of this effect was partly reduced by the typical achievable average ion currents of several tens of microamps. The ion storage lifetime was ≈80 s.

The absolute scale for the center-of-mass energy $E_{\rm cm}$ is calibrated using the electron beam energy. We measure the cathode voltage and the electron current simultaneously. In this way we are able to determine the space charge–corrected electron beam energy. Recently we have upgraded our method for measuring the beam voltage and current by adding a frequency-compensated high-voltage probe and a fast current-to-frequency converter (Nikolić et al. 2004; Kieslich et al. 2004). These enable simultaneous online monitoring of both the electron beam voltage and current. After correcting the electron energy in the laboratory frame by the electron space charge, $E_{\rm cm}$ is accurate to ±0.25%.

2.1. 2 → 2 *Measurements*

The $\Delta N = 0$ resonances were measured using a ±1 kV high-voltage amplifier to vary the electron beam energy. This amplifier has a fast response time and is floated on top of the power supply that provides the main cathode voltage and has a much slower response time.

DR measurements are carried out as a function of $E_{\rm cm}$ by varying the electron beam energy. The beam energy is chopped between cooling ($E_{\rm cool}$), measurement ($E_{\rm meas}$), and reference ($E_{\rm ref}$) energies, all measured in the lab frame. Data were collected using chopping patterns of $E_{\rm cool} - E_{\rm meas} - E_{\rm ref}$ and $E_{\rm cool} - E_{\rm ref} - E_{\rm meas}$.

The electron cooling force on the ions is effective only for very low relative velocities between the ions and electrons. At cathode voltages different from $E_{\rm cool}$, the ion beam can heat up due to intrabeam scattering. In order to reduce this effect, each chopping pattern included an electron beam energy setting of $E_{\rm cool}$ for 30 ms.

Typical measurement and reference energy dwelling times were set between 3 and 5 ms. Given a standard cooling energy dwelling time of 30 ms, each chopping cycle of three energy steps lasted about 40 ms. With typical ion lifetimes in the range of 80 s, several hundred chopping cycles could be made before new ion injections were needed to replace the ion current in the ring.

The measured recombined ion signal includes contributions due to DR, radiative recombination (RR), and charge transfer (CT) off the rest gas in the storage ring. Data collected at $E_{\rm ref} = E_{\rm cm} \approx 98$ eV are used to determine the recombined ion background due to CT for each chopping cycle. No significant DR resonances are expected at these energies. This allows us to determine the background signal rate for all energy steps.

When chopping the beam energy, the cathode voltage requires a certain settling time before it reaches the new desired value. This can result in voltage variations within a measurement window. The drifting of the voltage directly affects the measured width of the DR resonances. The amplitude of the voltage variation is proportional to the potential differences between $E_{\rm meas}$ and the preceding energy step. Resonance broadening can be reduced by avoiding large voltage differences between $E_{\rm meas}$ and the prior cooling or reference energy. Thus, at low relative energies a chopping sequence of $E_{\rm cool} - E_{\rm meas} - E_{\rm ref}$ was used and at high energies of $E_{\rm cool} - E_{\rm ref} - E_{\rm meas}$. For energies in between there is no ideal sequence.

2.2. 2 → 3 *Measurements*

The $\Delta N = 1$ resonances extend over a wide range that we were not able to cover using the high-voltage amplifier alone. To reach the necessary electron beam energies, after injection and cooling was complete, the main power supply was switched to the appropriate voltage. A limited energy subrange of the $\Delta N = 1$ resonances could then be covered using the high-voltage amplifier, floating atop the new electron cathode voltage. After collecting sufficient statistics for this limited energy range, we stopped the measurement and changed the voltage of the main power supply for the cathode. We then scanned over a new energy interval. By combining overlapping energy ranges, we were able to collect a complete spectrum of the $\Delta N = 1$ resonances. For the $\Delta N = 1$ data, it was not possible to cool the ions between each measurement step. This resulted in a portion of the resonance broadening in the measured data being due to heating up of the ion beam by intrabeam scattering.

2.3. *Metastable Ions*

In our measurements we detected metastable $^{56}Fe^{22+}$ ($1s^2 2s 2p\ ^3P_0^o$) ions in our beam by observing DR resonances due to the metastable parent ion. For beryllium-like ions with zero nuclear spin (such as ^{56}Fe), the $^3P_0^o$ level is forbidden to decay to the ground state via a one-photon transition and the multiphoton

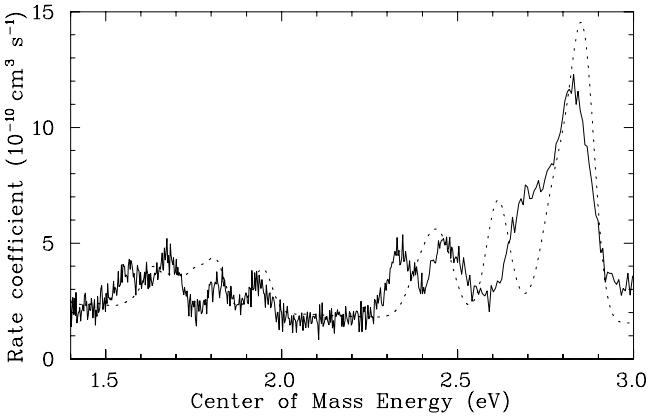

FIG. 1.— Fe XXIII to Fe XXII $2 \rightarrow 2$ DR resonance structure for E_{cm} from 1.4 to 3.0 eV. The data represent the DR and RR cross sections times the electron-ion relative velocity convolved with the energy spread of the experiment (i.e., the merged-beams rate coefficient $\langle v\sigma \rangle$) and are shown vs. electron-ion center-of-mass collision energy. All of the resonances in this energy range are attributed to metastable $^3P_0^o$ ions. The solid line shows our experimental results. The dotted line gives our calculated MCBP resonance structure for metastable ions multiplied by a factor of 0.07. We have added to our theoretical results the convolved, nonresonant RR contribution obtained from semiclassical calculations.

transition rate is negligible. Hence, this level can be considered as having a nearly infinite lifetime (Marques et al. 1993; Brage et al. 1998). It is not surprising then that we have detected these metastables in our measurement.

Assignment of the measured Fe^{22+} data to the ionic resonance structures was done with the help of multiconfiguration Breit-Pauli (MCBP) calculations, described in more detail below (§ 4.1), for both ground-state and $^3P_0^o$ metastable ions. In the energy region for DR due to $2 \rightarrow 2$ core excitations, the calculation for ground-state ions is largely dominated by the Rydberg series converging to the $2s^2\ ^1S_0 \rightarrow 2s2p\ ^1P_1^o$ excitation threshold. On the other hand, the calculated metastable spectrum shows a much less regular structure. In fact, most of the Rydberg resonances associated with the relevant $2s2p\ ^3P_0^o \rightarrow 2p^2$ excitations yield only very small DR cross sections as they strongly autoionize into the $2s2p\ ^3P_J^o$ continuum channels for $J = 1$ and 2, which are energetically open at collision energies of greater than 3.838 and 15.325 eV, respectively (using energies from the NIST database[4]).

In the measured spectrum we can identify eight resonances and/or resonance blends in the 1.40–2.95 eV energy range that arise exclusively from $^3P_0^o$ metastable parent ions. Using the quantum defects of Theodosiou et al. (1986), we assign the strongest of these to the $2p^2(^3P_1)9l$ ($l \geq 4$) resonance with a hydrogenic position at 2.89 eV. These eight features are well separated from any ground-state resonances (see Fig. 1). The resonance structure is fairly well reproduced, although not in all detail, by our MCBP calculations. This basic agreement, as well as the good agreement of the same calculation regarding the ground-state structures above 1 eV, led us to estimate the metastable fraction in the stored $^{56}Fe^{22+}$ ion beam by taking the ratio of the experimental and theoretical integrated resonance strengths in this energy range.

Our determination here may seem somewhat circular because it depends on the same theory that we are benchmarking. However, we note that for $^{56}Fe^{19+}$ we found good agreement between experiment and theory for $\Delta N = 0$ core excitations at collision energies above 1 eV. For MCBP calculations, the ratio of theoretical to experimental resonance strengths on average was 0.98 with a 1 σ scatter of ≈30%. Here we are using a number of resonances in our determination of the metastable fraction. This should help to reduce any effects due to the scatter in individual resonance strength ratios. But to err on the side of caution, we estimate that our metastable determination is good to about 30%. This yields a metastable fraction of 7% ± 2%. Thus, we conclude that uncertainties in our metastable fraction determination have an insignificant effect on our determination of the ground-state beam current.

This estimated metastable fraction seems to be in good agreement with that of Badnell et al. (1991) for their beams of beryllium-like C^{2+}, O^{4+}, and F^{5+}. They used a tandem accelerator to produce their ion beams for single-pass electron-ion merged-beams DR measurements. Their total $^3P_J^o$ ($J = 0, 1, 2$) metastable fraction was about 75%. Assuming that the various J levels in Badnell et al. (1991) were statistically populated, one would then expect that $^3P_0^o$ metastable ions would comprise $\frac{1}{9}$ of the total $^3P^o$ population or ≈8% of the ion beam current.

For our work we also used a tandem accelerator to produce beryllium-like ions. We stored the $^{56}Fe^{22+}$ ions in TSR. Then we cooled and waited a sufficient time (∼1 s) before beginning data acquisition. This allowed the $J = 1$ and 2 levels to decay away (using the NIST lifetimes),[5] leaving only the $J = 0$ level. If we now assume that our beam initially consisted of about 75% metastable $^3P_J^o$, then after about 1 s of storage time we would expect a beam with about 8% $J = 0$ metastable ions. This is in good agreement with the 7% ± 2% we have determined for $^{56}Fe^{22+}$.

We have reanalyzed our $2 \rightarrow 2$ data multiplying the measured ion current by a fraction of 0.93 to use the true ground-state ion current. For the $2 \rightarrow 3$ data, we did not make any such correction and used the full measured ion current in our data analysis. This is because at the high energies where the $2 \rightarrow 3$ channels are important, the contributions from the various $2l^2$ core configurations are expected to be roughly the same (e.g., Mitnik & Badnell 2004).

We close this section with a brief comment on the TSR $^{24}Mg^{8+}$ DR measurements of Schippers et al. (2004). As this is a zero nuclear spin beryllium-like ion, the $^{24}Mg^{8+}$ beam is expected to consist of both ground-state $^1S_0$ and metastable $^3P_0^o$ ions. Based on our $^{56}Fe^{22+}$ results, we expect an ≈7% metastable fraction in the $^{24}Mg^{8+}$ beam. However, no DR resonances due to this metastable parent ion were seen. This is most likely due to a combination of two effects. First is the opening up of additional autoionization channels as is explained above. The $e^- + 2s2p\ ^3P_0^o \rightarrow 2p^2nl$ capture channels can autoionize into the $2s2p\ ^3P_J^o$ ($J = 1, 2$) continuum for collision energies of more than 0.1397 and 0.4447 eV, respectively (using the NIST energies). Hence, we expect to see no significant metastable resonances in $^{24}Mg^{8+}$ for energies above ≈0.14 eV. Second is the fact that hydrogenic calculations of the $2p^2nl$ resonance energies indicate that there are no significant resonances in the 0–0.14 eV energy range. Thus, we can only estimate the $^{24}Mg^{8+}$ beam metastable component using our $^{56}Fe^{22+}$ results. Based on this, it is likely that the experimentally derived $^{24}Mg^{8+}$ DR rate coefficient of Schippers et al. (2004) should be shifted up by 7%. However, this is well within their estimated ±15% uncertainty and hence not necessary.

2.4. *Uncertainties*

Experimental uncertainties have been discussed in detail elsewhere (Kilgus et al. 1992; Lampert et al. 1996). The total

[4] Available at http://physics.nist.gov/asd3.

[5] See http://physics.nist.gov/cgi-bin/AtData/main_asd.

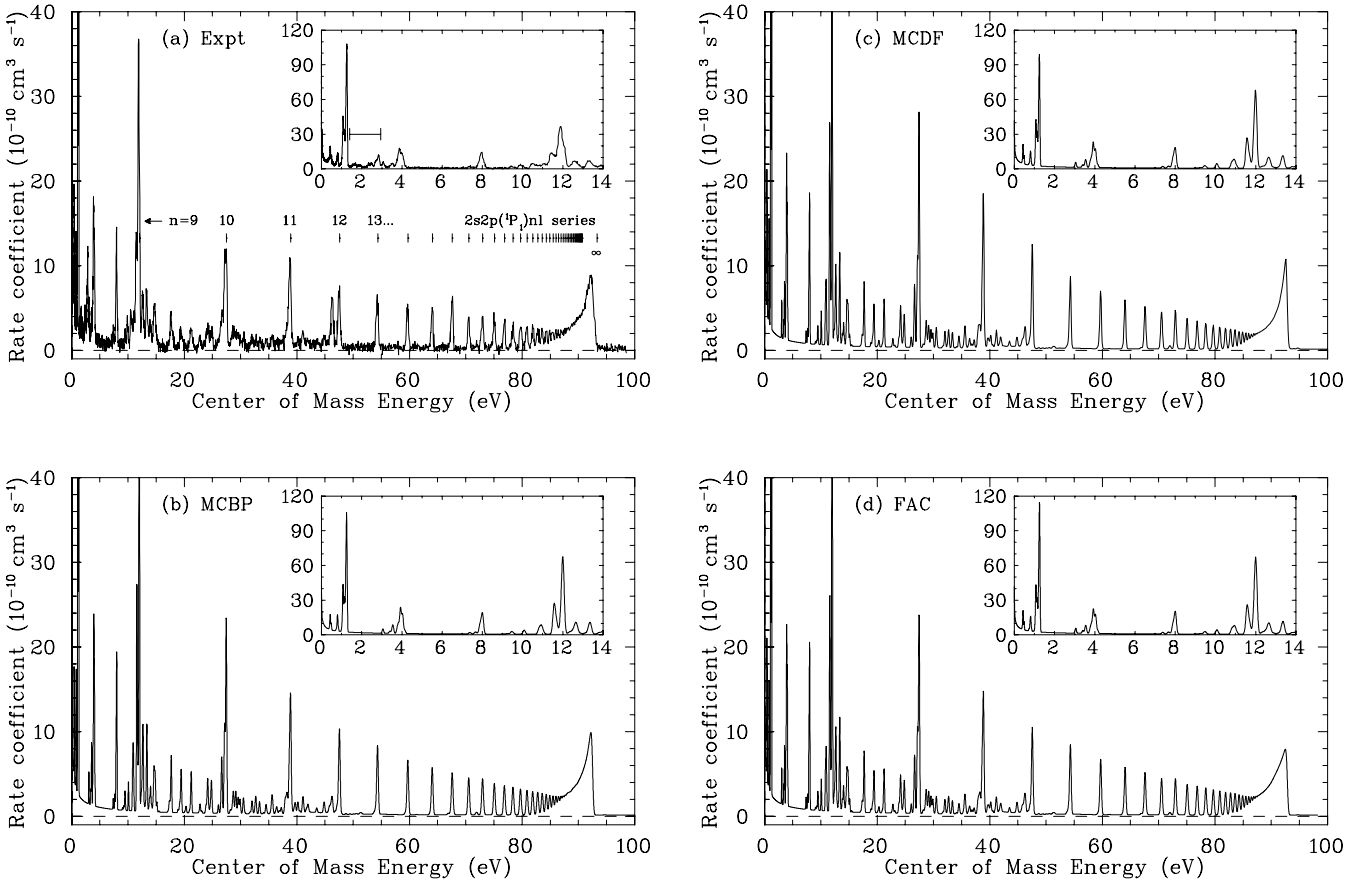

FIG. 2.—Fe XXIII to Fe XXII $2 \rightarrow 2$ DR resonance structure ($n_{max} = 118$): (*a*) experimental, (*b*) MCBP, (*c*) MCDF, and (*d*) FAC results. The experimental and theoretical data represent the DR and RR cross sections times the electron-ion relative velocity convolved with the energy spread of the experiment (i.e., the merged-beams rate coefficient $\langle v\sigma \rangle$) and are shown vs. electron-ion center-of-mass collision energy. In (*a*) resonances resulting from the $^1S_0 - ^1P_1$ core excitations are labeled for capture into high-*l* levels. Unlabeled resonances are due to capture into low-*l* levels or due to DR via other core excitations. The nonresonant "background" rate coefficient in (*a*) is due primarily to RR. The horizontal line in the inset of (*a*) shows the 1.40–2.95 eV energy range containing the resonances due to recombination onto metastable $^3P_0^o$ ions that were used to determine the metastable fraction of the ion beam (as is discussed in § 2.3 and shown in detail in Fig. 1). In (*b*), (*c*), and (*d*) the theoretical DR results have been multiplied by 0.93 for comparison purposes to take into account the 7% metastable contamination of our ion beam. Also in (*b*), (*c*), and (*d*), we have added to our DR results the convolved, nonresonant RR contribution obtained from semiclassical calculations.

systematic uncertainty in our absolute DR measurements is estimated to be $\lesssim$20%. The major sources of uncertainties include the electron beam density determination, the ion current measurement, corrections for the merging and demerging of the two beams, the efficiency of the recombined ion detector, resonance strength fitting uncertainties, and uncertainties in the shape of the interpolated smooth background (particularly in regions where the DR resonances were so numerous that the background was not directly observable). Another source of uncertainty is that we assume that each DR feature can be fitted using a single resonance peak when in fact each feature is often composed of many unresolved resonances. Relative uncertainties for comparing our DR results at different energies are estimated to be $\lesssim$10%. Uncertainties are quoted at a confidence level believed to be equivalent to a 90% counting statistics confidence level.

3. EXPERIMENTAL RESULTS

Our $2 \rightarrow 2$ and $2 \rightarrow 3$ DR resonance measurements are shown in Figures 2*a* and 3*a*, respectively. In Figure 2*a*, the data represent the sum of the RR and DR cross sections times the relative electron-ion velocity convolved with the energy spread of the experiment, i.e., the merged-beams rate coefficient $\langle v\sigma \rangle$. In Figure 3*a* the RR background has been subtracted out. The data in both figures are presented as a function of E_{cm}.

3.1. $2 \rightarrow 2$ *Resonances*

In Figure 2*a*, the strongest resonance series corresponds to $2s^2(^1S_0) \rightarrow 2s2p(^1P_1^o)$ core excitations. Many resonances are also seen due to other core excitations. Some of the smaller resonances below 3 eV are due to recombination of metastable Fe^{22+} $[2s2p(^3P_0^o)]$ ions (e.g., Fig. 1). We have carried out theoretical calculations (see §§ 2.3 and 4.1) to use as a guide to identify these resonances. Above $\approx$3 eV, there are no predicted significant DR resonances for metastable Fe^{22+}.

As discussed in § 2.1, for low relative energies we used a chopping pattern of $E_{cool} - E_{meas} - E_{ref}$. For $E_{cm} \lesssim 3$ eV, $E_{cool} \approx E_{meas}$ and any drift of the cathode voltage during the measurement window is minimal. This resulted in an effective energy spread associated with the relative motion between the ions and electrons corresponding to temperatures of $k_B T_\perp = 17$ meV perpendicular to the magnetic field confining the electron beam and $k_B T_\parallel = 0.15$ meV parallel to this magnetic field. Here k_B is Boltzmann's constant. For higher values of E_{cm} the drift becomes more important, broadening the measured resonances. For high relative energies we used $E_{cool} - E_{ref} - E_{meas}$, and for $E_{cm} \gtrsim 70$ eV broadening due to voltage drifting appears to be unimportant.

Due to the energy spread of the electron beam, resonances below $E_{cm} \approx k_B T_\perp \approx 17$ meV cannot be resolved from the near

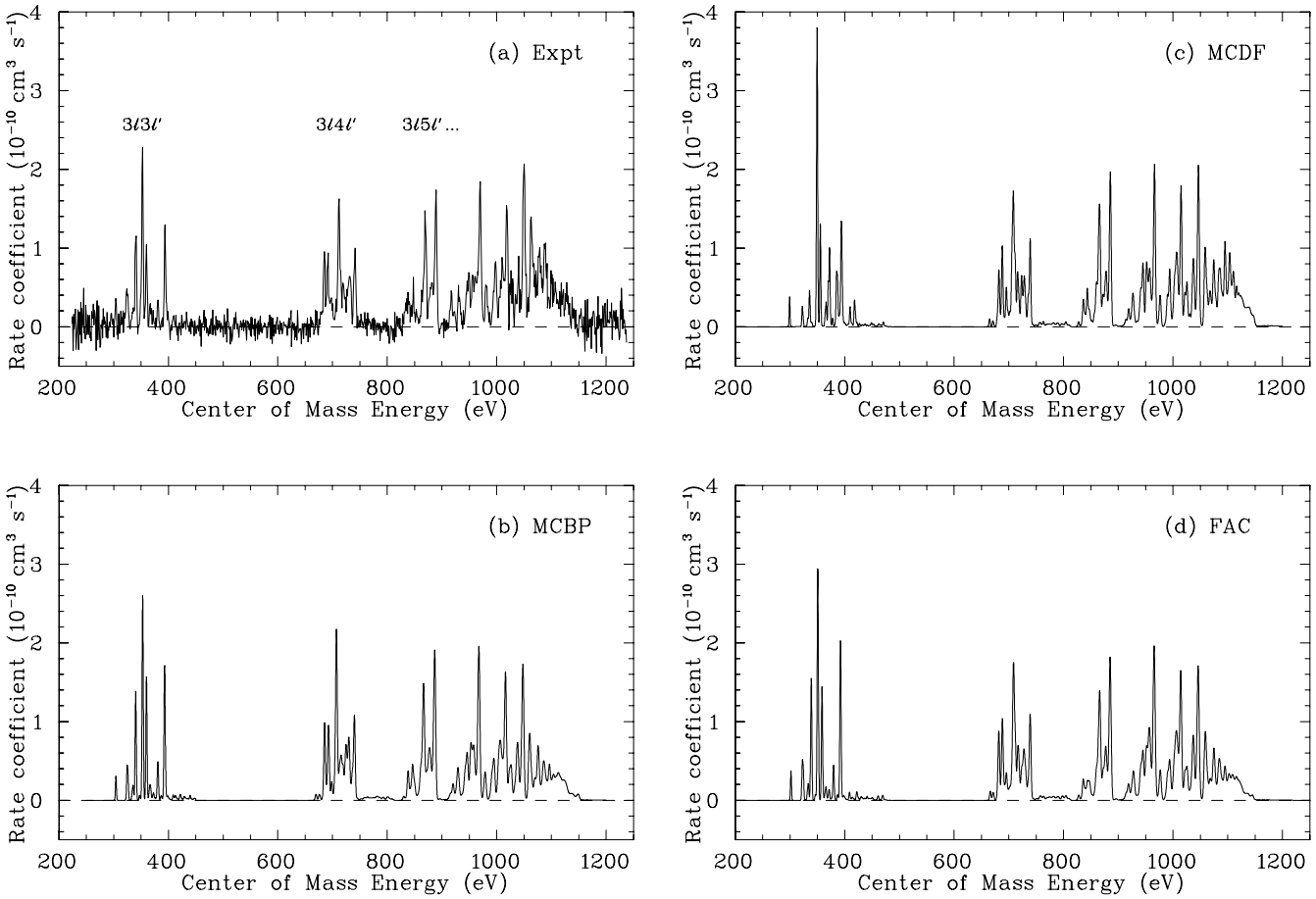

FIG. 3.—Fe XXIII to Fe XXII DR resonances due to $2 \rightarrow 3$ core excitations ($n_{max} = 118$): (*a*) experimental, (*b*) MCBP, (*c*) MCDF, and (*d*) FAC results. The experimental and theoretical data represent the DR cross section times the electron-ion relative velocity convolved with the energy spread of the experiment (i.e., the merged-beams rate coefficient $\langle \sigma v \rangle$). The data are shown vs. electron-ion collision energy. In (*a*) the measured DR resonances due to various $3lnl'$ doubly excited states are labeled. The nonresonant RR "background" has been subtracted in (*a*) and has not been included in (*b*), (*c*), and (*d*). The theoretical results have not been scaled to account for the metastable fraction in our ion beam for reasons discussed in § 3.3.

0 eV RR signal. However, we can infer that no significant resonances exist for either ground-state or metastable Fe^{22+}. At $E_{cm} \lesssim 10^{-4}$ eV, the measured recombination rate coefficient is a factor of only $\sim$2 larger than the RR rate coefficient predicted using semiclassical RR theory with quantum mechanical corrections (Schippers et al. 2001). This is comparable to the range of enhancement factors that has been found using electron coolers on storage rings for measurements of RR for bare ions (see Fig. 1 in Heerlein et al. 2002 and their references 2–12; see also Gwinner et al. 2000). Therefore, we believe that there are no unresolved DR resonances at energies $\lesssim$17 meV.

The lowest energy observed resonance occurs at a value of 0.0893 eV with a resonance strength of 3.1×10^{-19} cm^2 eV. This resonance was not seen in any of the theoretical calculations for either ground-state or metastable Fe^{22+}. Hence, it is not clear whether this resonance will or will not contribute to the total DR rate coefficient for ground-state Fe^{22+}.

3.2. $2 \rightarrow 3$ *Resonances*

The measured DR resonance structure for $2 \rightarrow 3$ DR of Fe XXIII is shown in Figure 3*a*. The spectrum is rich in resonance structure with many overlapping resonances within each manifold and between manifolds. The $3l3l'$, $3l4l'$, and $3l5l'$ manifolds are well separated in energy and easily identifiable. The higher $3lnl'$ ($n \geq 6$) manifolds overlap and are less easily identified. In addition, there are a number of weak $4l4l'$ resonances that lie between $\approx$1000 and 1240 eV and make a small contribution to the overall spectrum.

The energy resolution of the $2 \rightarrow 3$ DR measurements can be approximated by a Gaussian with an FWHM of

$$\Delta E_{FWHM} = 4(k_B T_{eff} E_{cm} \ln 2)^{1/2}, \quad (4)$$

where $k_B T_{eff}$ is the effective energy spread due to the combined energy spreads of the electron and ion beams. Due to blending of the DR resonances, we were unable to fit an individual DR resonance to determine the effective energy spread of the measurement. Instead, we estimated the energy spread using our theoretical results convolved with the energy spread of the experiment. For our MCBP and Flexible Atomic Code (FAC) calculations we used a Gaussian line shape. For our multiconfiguration Dirac-Fock (MCDF) results we used Voigt profiles. The Voigt functions account for the Lorentzian natural line shapes of the resonances and the Gaussian shape of the experimental energy spread. We found a best fit by eye of $k_B T_{eff} \approx 1.36$ meV.

3.3. *Rate Coefficients*

We have generated an experimentally derived rate coefficient for the sum of $2 \rightarrow 2$ and $2 \rightarrow 3$ DR of Fe XXIII forming Fe XXII in a plasma with a Maxwellian electron energy distribution. To produce a $2 \rightarrow 2$ rate coefficient, we have multiplied our $2 \rightarrow 2$

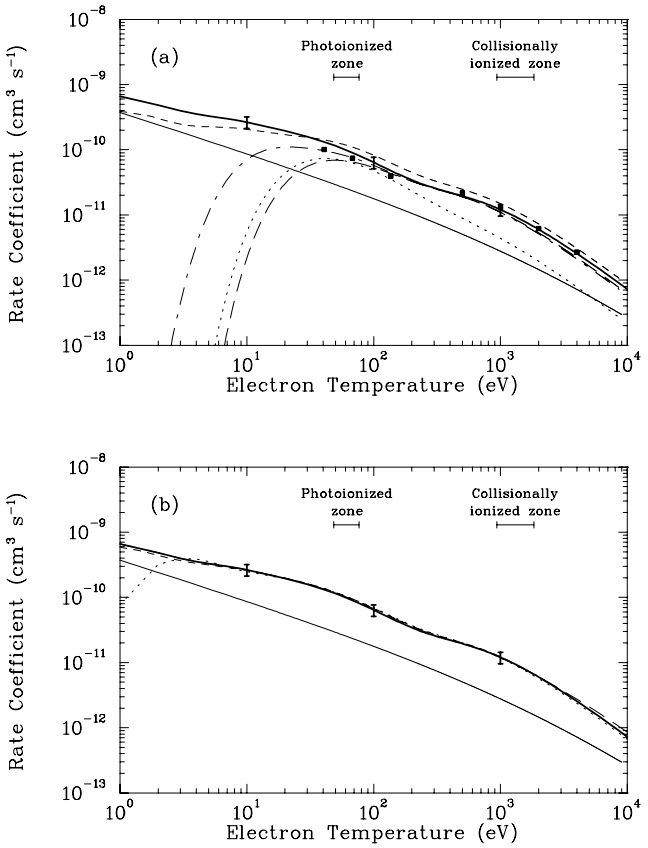

FIG. 4.—Fe XXIII to Fe XXII Maxwellian-averaged DR rate coefficient for recombination. (*a*) The thick solid line represents our experimentally derived rate coefficient using our $2 \rightarrow 2$ and $2 \rightarrow 3$ results ($n_{\max} = 118$). The thick error bars show our estimated total experimental uncertainty of $\lesssim$20%. Also shown are the published theoretical DR rate coefficients of Jacobs et al. (1977) as fitted by Shull & van Steenberg (1982; *dotted line*), the data of McLaughlin et al. (1987; *filled squares*), and the data of Romanik (1988; *short-dashed line*), as well as the recommended DR rate coefficients of Arnaud & Raymond (1992; *long-dashed line*) and Mazzotta et al. (1998; *dot-dashed line*), which are both based on the work of Badnell (1986). As a reference we give the recommended RR rate coefficient of Gu (2003a; *thin solid line*). (*b*) As in (*a*), the thick solid line represents our experimentally derived rate coefficient and the thin solid line the recommended RR rate. Also shown are our MCBP DR results for $n_{\max} = 1000$ (Colgan et al. 2003; *dotted line*), our MCDF results for $n_{\max} = 400$ (*short-dashed line*), and our FAC results for $n_{\max} = \infty$ (Gu 2003b; *long-dashed line*). All calculations include DR via $2 \rightarrow 2$ and $2 \rightarrow 3$ core excitations. On the scale of the figure, all three theoretical results overlap extremely well with our experimental results and at some temperatures are indistinguishable from the experimental curve. Neither the experimental nor theoretical DR rate coefficients in (*a*) or (*b*) include RR. The solid horizontal line shows the formation zone of Fe XXIII as predicted for an optically thin, low-density photoionized plasma of cosmic abundances (Kallman & Bautista 2001) and for low-density electron-ionized plasmas (Mazzotta et al. 1998).

DR data by a factor of 1/0.93 to account for the estimated 7% metastable contamination factor. In addition, we have excluded all resonances due to metastable ions (see, e.g., Fig. 1). For $2 \rightarrow 3$ DR the rate coefficients for the ground-state and metastable level are expected to be roughly the same (e.g., Mitnik & Badnell 2004). To calculate the experimentally derived $2 \rightarrow 3$ rate coefficient, we have therefore not corrected for the metastable fraction of the ion beam.

Figure 4 shows the resulting DR rate coefficient using the extracted resonance strengths for $E_{\rm cm} < 3.2$ eV and numerically integrating the higher energy data (after subtracting out the nonresonant background). Resonance strengths were extracted following the method outlined in Kilgus et al. (1992) and Lampert et al. (1996). The rate coefficient was calculated using the methodology outlined in Savin (1999) for resonance strengths and in Schippers et al. (2001) for numerical integration.

TABLE 1
FIT PARAMETERS

Parameter	Experiment[a]	Experiment[b]	MCDF
c_1	2.47E−6	7.48E−5	7.24E−5
c_2	1.21E−4	4.29E−5	4.12E−5
c_3	2.18E−3	1.98E−3	1.77E−3
c_4	1.50E−3	8.82E−4	1.36E−3
c_5	1.47E−2	8.01E−3	1.24E−2
c_6	3.14E−2	2.86E−2	3.08E−2
c_7	7.98E−2	8.36E−2	8.98E−2
c_8	1.25E−1	1.13E−1	1.11E−1
c_9	7.25E−1	7.43E−1	7.24E−1
E_1	8.93E−2	4.46E−1	4.40E−1
E_2	4.69E−1	5.17E−1	5.07E−1
E_3	1.16E+0	1.13E+0	1.12E+0
E_4	3.21E+0	2.16E+0	2.75E+0
E_5	1.04E+1	7.55E+0	9.53E+0
E_6	2.71E+1	1.96E+1	2.44E+1
E_7	7.82E+1	6.78E+1	7.39E+1
E_8	4.00E+2	3.50E+2	3.61E+2
E_9	9.88E+2	9.75E+2	9.62E+2

NOTES.—Fit parameters for the experimentally derived DR rate coefficient for Fe XXIII forming Fe XXII via $N = 2 \rightarrow N' = 2$ and $N = 2 \rightarrow N' = 3$ core excitation channels ($n_{\max} = 118$). Also given are the fit parameters for our calculated MCDF results ($n_{\max} = 400$). Fits for our MCBP and FAC data are given in Colgan et al. (2003) and Gu (2003b), respectively. The units are cm^3 s^{-1} K$^{1.5}$ for c_i and eV for E_i.

[a] Including the unidentified resonance at 0.0893 eV.

[b] Excluding the unidentified resonance at 0.0893 eV.

We estimate that the uncertainty in the absolute magnitude of our experimentally derived rate coefficient is $\lesssim$20% for $k_{\rm B}T_e > 0.001$ eV. Contributions due to DR into $n \geq n_{\max} = 118$ are estimated to have no effect for $k_{\rm B}T_e \leq 10$ eV. If included, these contributions would increase our summed DR rate by <6% for 10 eV $< k_{\rm B}T_e \leq 1000$ eV and by <2% above 1000 eV.

To take into account the uncertainty in whether or not the resonance at 0.0893 eV is due to ground-state or metastable Fe XXIII, we provide a fit to rate coefficients calculated with and without this resonance included. Actually the uncertainty of the parentage for this resonance is not expected to be an issue for plasma modeling. This resonance makes a significant contribution to the total DR rate coefficient only for $k_{\rm B}T_e < 0.2$ eV, and Fe XXIII is not predicted to form at these temperatures in either photoionized or electron-ionized plasmas (Mazzotta et al. 1998; Kallman & Bautista 2001).

We have fitted our experimentally derived rate coefficient using the simple fitting formula

$$\alpha_{\rm DR}(T_e) = T_e^{-3/2} \sum_i c_i e^{-E_i/k_{\rm B}T_e}, \qquad (5)$$

where c_i is the resonance strength for the ith fitting component and E_i is the corresponding energy parameter. Table 1 lists the best-fit values for the fit parameters. The fit including the low-energy resonance is good to better than 0.5% for 0.001 eV $\leq k_{\rm B}T_e \leq 10{,}000$ eV. The fit without this resonance is good to $\lesssim$0.5% for 0.1 eV $\leq k_{\rm B}T_e \leq 10{,}000$ eV. Below 0.1 eV, the fit goes to zero with decreasing T_e faster than the data. But this is not expected to be an issue as the total recombination rate coefficient at these temperatures is dominated by RR by orders of magnitude.

4. THEORY

Existing theoretical DR rate coefficients for Fe XXIII have been calculated using *LS* coupling by Jacobs et al. (1977), McLaughlin et al. (1987), and Romanik (1988). Badnell (1986) calculated $2 \rightarrow 2$ DR using the Burgess formula (Burgess 1965) and an MCBP method for $2 \rightarrow 3$ DR. All of these results are shown in Figure 4. However, there have been major theoretical and computational advances since this early DR work.

Recently, state-of-the-art theoretical results for Fe XXIII have been published by Colgan et al. (2003) and Gu (2003b) using two different theoretical methods. In addition, we have carried out new calculations using yet a third state-of-the-art theoretical technique. All of these methods use the independent processes and isolated resonance approximations (Seaton & Storey 1976). For Fe XXIII, we expect interference between DR and RR and the effects of interacting resonances to be unimportant (Pindzola et al. 1992). The DR cross section can then be written as a product of the resonance capture cross section (which is related by detailed balance to the autoionization rate) and the stabilizing radiative branching ratio. Below we briefly describe these techniques and the results.

4.1. *Multiconfiguration Breit-Pauli (MCBP)*

The theoretical details of the MCBP calculations have been reported in detail elsewhere (Badnell et al. 2003; Colgan et al. 2003). Briefly, the AUTOSTRUCTURE code was used to calculate energy levels and radiative and autoionization rates in the intermediate-coupling approximations. As previously mentioned, the rates are calculated in the isolated resonance approximation, which enables the generation of final-state level-resolved and total DR rate coefficients in the independent process approximation. The calculation includes the $2p^2$ configuration, which strongly mixes with the $2s^2$ configuration. Thus, recombination into $2p^2nl$ resonances, or trielectronic recombination (TR; Schnell et al. 2003), is included.

AUTOSTRUCTURE produces raw radiative rates (calculated here using the length gauge) and autoionization rates. These data must be postprocessed to obtain the final-state level-resolved and total DR rates. The ionic thresholds were shifted to known spectroscopic values for the $2 \rightarrow 2$ transitions. The AUTOSTRUCTURE calculations were performed with explicit n-values (in eqs. [2] and [3]) up to 118 in order to compare most closely with experiment. In Colgan et al. (2003) a quantum defect approximation was made for high-level values of n beyond 15. The minor differences in these two approaches have an insignificant effect on the resulting resonance strengths and Maxwellian rate coefficient.

For our present comparison between theory and experiment, we took into account radiative transitions between autoionizing states. Such transitions were not included in the previously calculated Maxwellian rate coefficients (Colgan et al. 2003), but we determine this to be a less than 5% effect on the total theoretical rate coefficient.

4.2. *Multiconfiguration Dirac-Fock (MCDF)*

In this work, DR was treated as a two-step process using an isolated resonance approximation. The target wave functions were obtained using an MCDF method (Grant et al. 1980), and the continuum wave functions were calculated in the distorted-wave approximation. The transition energies include contributions from the Breit interaction and quantum electrodynamic corrections (Grant et al. 1980). The Auger and radiative transition rates were evaluated using first-order perturbation theory (Chen 1985).

For Be-like ions, configuration interaction between $1s^22s^2\ {}^1S_0$ and $1s^22p^2\ {}^1S_0$ is quite strong. This results in significant two-electron excitation from the core with capture of the free electron to form a triply excited state. This TR process has been shown to produce recombination resonances and to induce a significant increase in the rate coefficients for $\Delta N = 0$ transitions in the low-temperature region for ions of lower charge states (Schnell et al. 2003). In the present work, the contributions from the TR processes were taken into account by performing MCDF calculations including configuration interaction from states with the same n complex.

For $\Delta N = 0$ transitions, explicit calculations were performed for intermediate states with $n \leq 39$ and $l \leq 12$. The resonance energies were adjusted using the known experimental excitation energies between $n = 2$ states from the NIST database. The contributions from higher n Rydberg states were included using an n^{-3} scaling for the appropriate Auger and radiative rates up to $n = 400$.

For $\Delta N \neq 0$ transitions, explicit calculations were carried out for $1s^22l3l'nl''$ intermediate states with $n \leq 21$ and $l'' \leq 9$. The same extrapolation procedure as in the $\Delta N = 0$ case was applied for these series. For the $1s^22l4l'nl''$ case, we included only $n \leq 5$ and $l'' \leq 4$ states because of their small contributions and fast convergence due to the opening of the $1s^22l3l'$ Auger channels. No energy adjustment was applied for the $\Delta N \neq 0$ DR transitions.

The radiative transition rates have been calculated using the velocity gauge. The use of the length gauge increases the high-n $\Delta N = 0$ DR strengths by ≈10%–15%. It also increases the $3l3l'$ DR resonance strengths by ≈30% and the $3lnl'$ ($n \geq 8$) resonance strengths by ≈40%. The effects on the other DR channels are only a few percent. Lastly, a one-step cascade correction was applied to the DR calculations if the radiative decay to the autoionizing state was a major decay branch.

4.3. *Flexible Atomic Code (FAC)*

FAC is a relativistic, configuration interaction program for calculating various atomic collisional and radiative processes, including radiative transition rates (calculated here using the length gauge) and autoionization rates. These rates are needed to obtain DR cross sections. The single-electron basis wave functions are constructed using an optimized local central potential. Configuration interaction within the same complexes (configurations having the same set of principle quantum numbers) are included in deriving the atomic state wave functions. TR via $1s^22p^2$ core excitations, which is simply a configuration interaction effect, is thus naturally included. Both autoionization and radiative transition rates are evaluated in the first-order perturbation theory.

The calculations presented here use the same method as Gu (2003b). For the $2 \rightarrow 2$ core excitation channels, explicit calculations are performed for the resonances with $n \leq 50$ and $l \leq 12$. For the $2 \rightarrow 3$ DR channels, explicit calculations are performed for $n \leq 20$ and $l \leq 8$. For both channels, contributions from higher n resonances are taken into account using the hydrogenic scaling laws of autoionization and radiative transition rates. For the $2 \rightarrow 2$ channels, the resonance energies are empirically adjusted using the experimental excitation energies of $2 \rightarrow 2$ transitions of Fe XXIII.

In the calculation of radiative stabilizing branching ratios, cascades to autoionizing states are fully taken into account using an iterative procedure:

$$B_i = \frac{\sum_j A^r_{ij} + \sum_{i'} A^r_{ii'} B_{i'}}{\sum_j A^a_{ij} + \sum_k A^r_{ik}}, \tag{6}$$

TABLE 2
Integrated Resonance Strengths

Dominant Complex	E_{min} (eV)	E_{max} (eV)	$\int_{E_{min}}^{E_{max}} \sigma_{DR}\, dE$ (10^{-18} cm^2 eV) Expt	MCBP	MCDF	FAC	Ratio MCBP/Expt	MCDF/Expt	FAC/Expt
$3l3l'$	250	600	2.74	2.45	2.77	2.70	0.894	1.01	0.985
$3l4l'$	600	825	2.03	2.34	2.23	2.30	1.15	1.10	1.13
$3l5l'$	825	900	1.55	1.67	1.63	1.54	1.08	1.05	0.994
$3l6l'$	900	975	1.47	1.40	1.43	1.49	1.05	0.973	1.01
$3l7l'$	975	1023	1.19	1.12	1.17	1.17	0.941	0.983	0.983
$3lnl'$ ($n \geq 8$)	1023	1236	3.51	2.22	3.11	2.19	0.632	0.886	0.624

Notes.—Integrated resonance strengths for selected energy ranges of the $2 \rightarrow 3$ DR resonances shown in Figs. 3*a*–3*d*. Listed are the dominant resonance complex for each energy range; the limits of integration E_{min} and E_{max}; the integrated experimental, MCBP, MCDF, and FAC resonance strengths; and the ratio of the MCBP, MCDF, and FAC results to the experimental results. Adding the contributions above ~1000 eV due to the $4l4l'$ resonances would increase the theoretical integrated resonance strengths by $\sim 0.4 \times 10^{-18}$ cm^2 eV.

where A^r_{ij} is the radiative decay rate from state i to state j and A^a_{ik} is the autoionization rate from state i to state k. State i' may further autoionize and has a stabilizing branching ratio of $B_{i'}$.

4.4. *Results*

For the MCBP, MCDF, and FAC results, the DR cross section was approximated by the sum of Lorentzian profiles for all included resonances. This analytic cross section was convolved with the experimental energy resolution for comparison with the measured results. The convolved results are presented for $2 \rightarrow 2$ core excitations in Figures 2*b*–2*d* and for $2 \rightarrow 3$ core excitations in Figures 3*b*–3*d*. The results all use an $n_{max} = 118$.

Total $2 \rightarrow 2$ plus $2 \rightarrow 3$ DR rate coefficients were obtained by convolving the DR cross section with a Maxwellian electron energy distribution. The resulting Maxwellian rate coefficients are given in Figure 4*b*. MCBP, MCDF, and FAC results are given for $n_{max} = 1000$, 400, and ∞, respectively.

Fits for the total $2 \rightarrow 2$ plus $2 \rightarrow 3$ DR rate coefficient for the MCBP and FAC results have been given by Colgan et al. (2003) and Gu (2003b), respectively. Here we have fitted the theoretical MCDF DR rate coefficients using equation (5). Fit parameters are given in Table 1. The fit is given for an $n_{max} = 400$. Contributions due to higher n levels are expected to have an insignificant effect on the total DR rate coefficient. The accuracy of the MCDF fit is better than 1.3% for the temperature range 0.02 eV $\leq k_B T_e \leq$ 10,000 eV. With decreasing temperature below 0.02 eV, the fit goes to zero faster than the calculated rate coefficient. But this is not expected to be a problem for plasma modeling as it is extremely unlikely that Fe XXIII will ever form below this temperature (Mazzotta et al. 1998; Kallman & Bautista 2001). Also, RR is expected to dominate the total electron-ion recombination rate coefficient at these low temperatures.

5. DISCUSSION

5.1. *Resonance Structure*

In general, we find for the $2 \rightarrow 2$ DR resonances that the experimental and theoretical resonance strengths agree to within approximately ±20% for all of the strong complexes. This can be seen, in part, in Figures 2*a*–2*d*. Note that in these figures the differences between the experimental and theoretical resonance amplitudes for energies 3 eV $\lesssim E_{cm} \lesssim$ 70 eV are largely due to the changing experimental energy spread. This broadens the measured resonances and reduces the peak amplitude. But the actual integrated experimental resonance strengths show the agreement with theory noted above. This broadening appears not to be significant for energies above ≈70 eV where we were using an $E_{cool} - E_{ref} - E_{meas}$ chopping pattern.

One discrepancy between theory and experiment worth noting is the relatively strong peak at ≈46 eV that is underestimated by the various calculations. This is the $e^- + 2s^2\ {}^1S_0 \rightarrow 2p^2({}^1D_2)8l$ TR resonance. The MCBP, MCDF, and FAC integrated resonance strengths for this peak are only ≈40%–45% of the experimental value. It should be noted that theory sometimes tends to underestimate the resonance strength for TR (e.g., Schnell et al. 2003).

A comparison between our experimental and theoretical results for $2 \rightarrow 3$ DR is given in Table 2 and in Figures 3*a*–3*d*. Again, overall we find good agreement between experiment and theory, typically to within approximately ±20%. The largest differences between theory and experiment show up in the $3lnl'$ ($n \geq 8$) complex. The MCBP and FAC results both significantly underestimate the integrated resonance strength for this complex. The MCDF results slightly underestimate the integrated resonance strength. None of the calculations include the contributions from the $4l4l'$ resonances due to $2 \rightarrow 4$ core excitations. Adding this $\sim 0.4 \times 10^{-18}$ cm^2 eV contribution to the theory slightly reduces the difference between the MCBP and FAC results with experiment but does not remove it. Adding the $4l4l'$ contributions to the MCDF results removes the difference with experiment.

5.2. *Rate Coefficients*

Previously, DR rate coefficients have been calculated using *LS* coupling by Jacobs et al. (1977), McLaughlin et al. (1987), and Romanik (1988). These are shown in Figure 4*a*. We find poor agreement between our experimentally derived rate coefficient and the results of Jacobs et al. (1977). There is reasonable agreement with the calculations of McLaughlin et al. (1987) over the energy range for which they presented results. We also find reasonable agreement with the data of Romanik (1988).

Badnell (1986) produced a DR rate coefficient using the Burgess formula for the $2 \rightarrow 2$ channel and MCBP method for the $2 \rightarrow 3$ channel. The fits by Arnaud & Raymond (1992) and Mazzotta et al. (1998) to these results are shown in Figure 4*a*. However, their fits appear to be valid only for temperatures above ≈100 eV, as can be seen by comparing their results with the data in Figure 1 of Badnell (1986). Above ≈100 eV, there is good agreement between the fits to the data of Badnell (1986) and our experimentally derived rate coefficient.

A comparison between our experimental results and state-of-the-art DR calculations is given in Figure 4*b*. For temperatures above 3 eV, we find good agreement between the experimental

results and our MCBP, MCDF, and FAC results. Below 3 eV the MCBP rate coefficient drops off due to a slight inaccuracy in the fits used in Colgan et al. (2003) to model the actual rate coefficient. In these fits only five terms were kept in the expansion of equation (5). By adding another term to this expansion, a fitted rate coefficient is generated that is very close to the experimental results. Updated fit parameters can be found online.[6]

Agreement between our experimentally derived DR rate coefficient and MCBP, MCDF, and FAC results is good to within ≈20% over the temperature range predicted to be relevant for Fe XXIII in photoionized gas (Kallman & Bautista 2001) and electron-ionized gas (Mazzotta et al. 1998). These temperature spans cover the range where the fractional Fe XXIII abundance is greater than 10% of the total Fe abundance. A similar temperature range selection criterion was used in Savin et al. (1997, 1999, 2002a, 2002b, 2003).

None of the calculations include the effects of the $4l4l'$ resonances in their calculated rate coefficient. These resonances are naturally included in the TSR measurements. Our experimentally derived DR rate coefficient shows that the effects of omitting these resonances from the calculations are not significant.

5.3. *Implications for Plasma Modeling*

Our experimental results show that modern DR theory is able to produce reliable rate coefficients for high-Z ions such as Fe XXIII at the low temperatures relevant for photoionized gas and at the high temperatures relevant for electron-ionized gas. The work of Schippers et al. (2004), however, showed that while there was good agreement between modern DR theory and experiment for high-temperature DR of the moderate-Z ion Mg IX, such was not the case for the low temperatures relevant for photoionized gas. At these lower temperatures a significant discrepancy was found.

The reason for this discrepancy is a combination of the temperature at which an ion forms in photoionized gas and the resonances that dominate the DR process at that temperature. In a given isoelectronic sequence, high-Z ions are formed at higher temperatures than are moderate- or low-Z ions. For the higher Z ions, uncertainties in the energies of the important resonances are a small fraction of the total resonance energy E_d. The effect is thus small on the resulting Maxwellian rate coefficient, which contains an $\exp(-E_d/k_{\rm B}T_e)$ term. For moderate- to low-Z ions, this fractional uncertainty is larger and can have a more significant effect on the exponential term when calculating the theoretical DR rate coefficient.

Additional problems involve the question of whether a state is bound or not. Resonance energy uncertainties can lead to theory predicting that a doubly excited state lies in the continuum and contributes to the DR process when it is actually bound and does not. This can lead to theory overestimating the DR rate coefficient, or theory might calculate that a state is bound when it is actually autoionizing, thereby leading to an underestimation of the DR rate coefficient.

Probably the single greatest challenge facing modern DR theory is accurately calculating the resonance structure for the low collision energies needed to calculate low-temperature DR. As explained above, it is for these resonances that the energy uncertainties have the greatest effects on the predicted rate coefficient. So, unless there are significant advances in atomic structure calculations soon, astrophysicists are going to have to continue to rely on storage ring measurements in order to generate accurate low-temperature DR rate coefficients for those moderate- to low-Z ions that have important DR resonances at collision energies comparable to the temperature where the ion forms in photoionized gas.

[6] See http://amdpp.phys.strath.ac.uk/tamoc/DR.

We would like to thank A. Rasmussen for stimulating discussions and the excellent support given by the MPI-K accelerator and TSR crews. This work was supported in part by the NASA Space Astrophysics Research and Analysis program and the NASA Solar Physics Research, Analysis, and Suborbital program. Work performed in Germany has been supported in part by the German Federal Minister for Education and Research (BMBF) under contracts 06 GI 475, 06 GI 848, and 06 HD 854I and the German Research Council (DFG, Bonn-Bad Godesberg) under project MU 1068/8. Work performed at Lawrence Livermore National Laboratory was carried out under the auspices of the US Department of Energy by the University of California, Lawrence Livermore National Laboratory, under contract W-7405-ENG-48. M. F. G. is supported by NASA Astronomy and Physics Research and Analysis grant NAG5-5419. Part of this work was performed under the auspices of the US Department of Energy at Los Alamos National Laboratory.

REFERENCES

Arnaud, M., & Raymond, J. 1992, ApJ, 398, 394
Badnell, N. R. 1986, J. Phys. B, 19, 3827
Badnell, N. R., Pindzola, M. S., Andersen, L. H., Bolko, J., & Schmidt, H. T. 1991, J. Phys. B, 24, 4441
Badnell, N. R., et al. 2003, A&A, 406, 1151
Brage, T., Judge, P. G., Aboussaïd, A., Goderfroid, M. R., Jönsson, P., Ynnerman, A., Frose Fischer, C., & Leckrone, D. S. 1998, ApJ, 500, 507
Brickhouse, N. S., Raymond, J. C., & Smith, B. W. 1995, ApJS, 97, 551
Burgess, A. 1965, ApJ, 141, 1588
Chen, M. H. 1985, Phys. Rev. A, 31, 1449
———. 2002, Phys. Rev. A, 66, 052715
Colgan, J., Pindzola, M. S., Whiteford, A. D., & Badnell, N. R. 2003, A&A, 412, 597
DeWitt, D. R., Schuch, R., Gao, H., Zong, W., Asp, S., & Biedermann, C. 1996, Phys. Rev. A, 53, 2327
Ferland, G. J. 2003, ARA&A, 41, 517
Ferland, G. J., Korista, K. T., Verner, D. A., Ferguson, J. W., Kingdon, J. B., & Verner, E. M. 1998, PASP, 110, 761
Fogle, M., Badnell, N. R., Glans, P., Loch, S. D., Madzunkov, S., Abdel-Naby, Sh. A., Pindzola, M. S., & Schuch, R. 2005, A&A, 442, 757
Grant, I. P., McKenzie, B. J., Norrington, P. H., Mayers, D. F., & Pyper, N. C. 1980, Comput. Phys. Commun., 21, 207
Gu, M. F. 2003a, ApJ, 589, 1085
———. 2003b, ApJ, 590, 1131
Gwinner, G., et al. 2000, Phys. Rev. Lett., 84, 4822
Heerlein, C., Zwicknagel, G., & Toepffer, C. 2002, Phys. Rev. Lett., 89, 083202
Jacobs, V. L., Davis, J., Kepple, P. C., & Blaha, M. 1977, ApJ, 211, 605
Kallman, T. R., & Bautista, M. 2001, ApJS, 133, 221
Kenntner, J., et al. 1995, Nucl. Instrum. Methods Phys. Res. B, 98, 142
Kieslich, S., et al. 2004, Phys. Rev. A, 70, 042714
Kilgus, G., Habs, D., Schwalm, D., Wolf, A., Badnell, N. R., & Müller, A. 1992, Phys. Rev. A, 46, 5730
Lampert, A., Wolf, A., Habs, D., Kilgus, G., Schwalm, D., Pindzola, M. S., & Badnell, N. R. 1996, Phys. Rev. A, 53, 1413
Marques, J. P., Parent, F., & Indelicato, P. 1993, Phys. Rev. A, 47, 929
Mazzotta, P., Mazzitelli, G., Colafrancesco, S., & Vittorio, N. 1998, A&AS, 133, 403
McLaughlin, D. J., LaGattuta, K. J., & Hahn, Y. 1987, J. Quant. Spectrosc. Radiat. Transfer, 37, 47
Mewe, R., Gronenschild, E. H. B. M., & van den Oord, G. H. J. 1985, A&AS, 62, 197
Mitnik, D. M., & Badnell, N. R. 2004, A&A, 425, 1153
Mohamed, T., Nikolić, D., Lindroth, E., Madzunkov, S., Fogle, M., Tokman, M., & Schuch, R. 2002, Phys. Rev. A, 66, 022719

Müller, A. 1995, At. Plasma Material Interactions, 6, 59
Nikolić, D., et al. 2004, Phys. Rev. A, 70, 062723
Pindzola, M. S., Badnell, N. R., & Griffin, D. C. 1992, Phys. Rev. A, 46, 5725
Romanik, C. J. 1988, ApJ, 330, 1022
Savin, D. W. 1999, ApJ, 523, 855
———. 2000, ApJ, 533, 106
Savin, D. W., & Laming, J. M. 2002, ApJ, 566, 1166
Savin, D. W., et al. 1997, ApJ, 489, L115
———. 1999, ApJS, 123, 687
———. 2000, in AIP Conf. Proc. 547, Atomic Processes in Plasmas, ed. R. C. Mancini & R. A. Phaneuf (New York: AIP), 267
———. 2002a, ApJ, 576, 1098
———. 2002b, ApJS, 138, 337
———. 2003, ApJS, 147, 421
Schennach, M., et al. 1994, Z. Phys. D At. Mol. Clusters, 30, 291
Schippers, S., Bartsch, T., Brandau, C., Gwinner, G., Linkemann, J., Müller, A., Saghiri, A. A., & Wolf, A. 1998, J. Phys. B, 31, 4873
Schippers, S., Müller, A., Gwinner, G., Linkemann, J., Saghiri, A. A., & Wolf, A. 2001, ApJ, 555, 1027
Schippers, S., Schnell, M., Brandau, C., Kieslich, S., Müller, A., & Wolf, A. 2004, A&A, 421, 1185
Schippers, S., et al. 2000, Phys. Rev. A, 62, 022708
Schnell, M., et al. 2003, Phys. Rev. Lett., 91, 043001
Seaton, M. J., & Storey, P. J. 1976, in Atomic Processes and Applications, ed. P. G. Burke & B. L. Moisewitch (Amsterdam: North-Holland), 133
Shima, K., Kuno, N., Yamanouchi, M., & Tawara, H. 1992, At. Data Nucl. Data Tables, 51, 173
Shull, J. M., & van Steenberg, M. 1982, ApJS, 48, 95 (erratum 49, 351)
Theodosiou, C. E., Inokuti, M., & Manson, S. T. 1986, At. Data Nucl. Data Tables, 35, 473
Zatsarinny, O., Gorczyca, T. W., Korista, K. T., Badnell, N. R., & Savin, D. W. 2003, A&A, 412, 587